

Optimizing Winograd Convolution on ARMv8 processors

HAOYUAN GUI, XIAOYU ZHANG, CHONG ZHANG, and ZITONG SU, Institute of Software, Chinese Academy of Sciences China; Also at University of Chinese Academy of Sciences, China

HUIYUAN LI, Institute of Software, Chinese Academy of Sciences; Also at State Key Laboratory of Computer Science, Chinese Academy of Sciences, China

As Convolutional Neural Networks (CNNs) gain increasing prominence in deep learning, algorithms such as Winograd Convolution have been introduced to boost computational efficiency. However, existing Winograd implementations often face challenges, including significant transformation overhead, suboptimal computation efficiency, and reduced parallel performance in certain layers. In this work, we propose a fused Winograd Convolution algorithm tailored for ARMv8 CPUs, integrating the three core stages—input and filter transformation, computation, and output transformation—into a single pipeline. By maintaining consecutive memory access where possible and packing data in a custom z-shaped layout, our approach fully exploits a meticulously optimized GEMM micro-kernel that employs a ping-pong technique. Furthermore, we introduce a novel multi-dimensional parallel strategy that adaptively determines which dimensions to parallelize based on the scale of the convolutional layers, thereby addressing inefficiencies found in existing methods. To further boost performance, we manually optimize each kernel in AArch64 assembly, carefully tuning blocking parameters for the ARMv8 architecture to minimize transformation overhead and maximize computational throughput. Experimental results demonstrate that our method achieves up to 4.74 \times , 4.10 \times , 4.72 \times , and 10.57 \times speedups over NCNN, NNPACK, FastConv, and ACL, respectively, on the Kunpeng 920 platform when using multiple threads, with corresponding gains of 3.85 \times , 2.81 \times , 4.20 \times , and 7.80 \times on the AWS Graviton2, and 3.32 \times , 3.68 \times , 8.00 \times , and 9.28 \times on the Phytium 2000+.

CCS Concepts: • **Computing methodologies** → **Parallel computing methodologies**; **Artificial intelligence**.

Additional Key Words and Phrases: ARMv8 architectures, convolution, optimization, SIMD

1 INTRODUCTION

Convolutional Neural Networks (CNNs) have achieved great advancements and demonstrated exceptional performance across various fields of artificial intelligence [9, 16, 23, 26, 28]. Despite their impressive accuracy and versatility, CNNs require substantial computational resources, primarily due to the computational intensive operations within their convolutional layers. As CNN models continue to grow in complexity and depth, the need for efficient optimization techniques becomes increasingly critical.

Lavin and Gray [19] proposed leveraging the Winograd minimal filtering algorithm [33] to mitigate the computational complexity inherent in convolution operations. This efficient algorithm divides the input of convolutional networks into numerous tiles, transforms these tiles and the corresponding filters into the Winograd domain, performs element-wise multiplications, and subsequently transforms the results back into the spatial domain. This approach reduces the number of arithmetic operations required, thereby enhancing the computational efficiency of convolutional neural networks. Consequently, it has been incorporated into contemporary deep learning libraries. For instance, CuDNN [1] and MIOPEN [15] have implemented Winograd-based convolution for Nvidia GPUs and AMD GPUs, respectively. Similarly, OneDNN [12] and FALCON [24] have implemented this approach for x86 CPUs. Additionally, libraries such

Authors' addresses: HAOYUAN GUI, guihaoyuan123@icloud.com; XIAOYU ZHANG, zhangxy420@foxmail.com; CHONG ZHANG, zhangchong2020@iscas.ac.cn; ZITONG SU, suzitong21@gmail.com, Institute of Software, Chinese Academy of Sciences China; Also at University of Chinese Academy of Sciences, No. 4, Zhong-Guan-Cun South-4th St., Haidian District, Beijing, 100190, China; HUIYUAN LI, huiyuan@iscas.ac.cn, Institute of Software, Chinese Academy of Sciences; Also at State Key Laboratory of Computer Science, Chinese Academy of Sciences, No. 4, Zhong-Guan-Cun South-4th St., Haidian District, Beijing, 100190, China.

as NCNN [30], NNPACK [5], FastConv [22] and the ARM Compute Library (ACL) [6] have been designed specifically for ARM CPUs. ARM architecture, which predominates in the mobile computing domain, is also making significant inroads into high-performance computing (HPC) systems and has become a popular choice for convolution training and inference.

Although Winograd convolution is efficient, its implementation on ARM architecture remains a long-term challenge. Our observations indicate that current implementations on ARM still exhibit several technical issues that need to be addressed, including the following:

- Most current implementations treat input transformation, matrix multiplication, and output transformation as separate stages or only partially fuse these stages. Consequently, they fail to fully exploit cache locality.
- While Winograd convolution can be mapped onto General Matrix Multiplication (GEMM) to leverage higher arithmetic intensity, this approach incurs additional transformation overhead, primarily due to strided memory access. ARM-based implementations (e.g., NCNN, FastConv, and NNPACK) often use ARM NEON intrinsics [4] for the transformation kernels, but these intrinsics-based methods do not sufficiently reduce overhead compared to hand-optimized assembly. Although assembly development is more complex, it affords deeper architectural control and potentially greater performance gains.
- The data layout in current GEMM-based implementations generally considers only blocking for storing transformed matrices, limiting further optimization opportunities.
- The parallel strategies used by some implementations are not specifically tuned for individual convolutional layers, resulting in suboptimal parallelization.

In response to these limitations, we present several novel contributions and improvements in our work, as follows:

- We present a novel fused Winograd Convolution algorithm that couples the input transformation, matrix multiplication, and output transformation. This approach requires only a relatively small memory space to store temporary results, thereby better utilizing cache locality and reducing Translation Lookaside Buffer (TLB) misses.
- We propose two methods to implement the transformation kernel, which can reuse the data and save the load operations and fused-multiply-add (FMA) instructions.
- We implement all micro-kernels (both transformation and GEMM) using AArch64 assembly for ARMv8, enabling software prefetching instructions to mitigate strided memory-access overhead. This also provides tighter control over registers and minimizes the unpredictability of compiler optimizations, thereby improving resource utilization and performance.
- We employ a ping-pong technique to develop an optimized GEMM micro-kernel and design a specialized data layout to store transformed matrices in a GEMM-friendly format. This ensures continuous memory access throughout the micro-kernel execution. As a result, our method achieves up to 94.81% of the Kunpeng 920's theoretical peak performance under single-core execution.
- We perform a thorough performance modeling study to determine optimal block parameters for our approach, thereby reducing edge-case occurrences and enhancing overall throughput.
- We propose a multi-dimensional parallel strategy, specifically adapted to our fused framework, that enhances parallel efficiency across convolutional layers of varying scales. This approach delivers more robust and balanced improvements than other state-of-the-art libraries throughout our benchmark layers.

By applying these optimizations, our method achieves up to 4.74×, 4.10×, 4.72×, and 10.57× speedups over NCNN, NNPACK, FastConv, and ACL respectively using multiple threads on the Kunpeng 920 platform, 3.85×, 2.81×, 4.20×, and 7.80× on the AWS Graviton2, and 3.32×, 3.68×, 8.00×, and 9.28× on the Phytium 2000+ platform.

The remainder of this paper is organized as follows: Section 2 provides the background of Winograd Convolution. Section 3 details our system design framework, including the kernels for transformation and GEMM, as well as the design of the parallel strategy. Section 4 evaluates the performance of our approach in comparison to NCNN, NNPACK, FastConv and ACL. Section 5 discusses related work on Winograd Convolution, and Section 6 concludes the paper and discusses future research directions.

2 BACKGROUND

2.1 Convolution Neural Networks

In a convolution neural network layer, a filter tensor F with the dimensions $K \times C \times R \times S$ is applied to an input tensor D which is shaped $N \times C \times H \times W$. In this context, K and C represent the number of output and input channels, respectively. The dimensions R and S (resp. H and W) correspond to the height and width of the filter (resp. input). Finally, N denotes the batch size of the input. For the following equation, each element of F and D is denoted as $F_{k,c,u,v}$ and $D_{b,c,i,j}$, respectively. The corresponding output tensor O for the b -th batch and k -th output channels can be calculated by Equation (1),

$$O_{b,k,i,j} = \sum_{c=1}^C \sum_{u=1}^R \sum_{v=1}^S D_{b,c,i+u,j+v} \cdot F_{k,c,u,v}. \quad (1)$$

Thus, it can also be rewritten as

$$O_{b,k} = \sum_{c=1}^C D_{b,c} * F_{k,c}. \quad (2)$$

where $*$ denotes convolution operation.

2.2 Winograd Convolution

Winograd convolution [19] leverages the Winograd minimal filtering algorithm [33] to reduce arithmetic complexity of the convolution process. The notation $F(m, r)$ represents using an r -tap FIR filter to compute m outputs, where the input size is $m + r - 1$. This method can reduce the number of multiplications by a factor of $(m \times r) / (m + r - 1)$ compared to the direct convolution. For n -dimensional, this notation extends to $F(m_1 \times m_2 \times \dots \times m_n, r_1 \times r_2 \times \dots \times r_n)$, where the length of output and filter in the i -th dimension are m_i and r_i , respectively.

To illustrate, we use 2-D convolution as an example. Winograd convolution employs overlap-add (OLA) method, splitting $D_{b,c}$ with dimensions $H \times W$ into $[(H - r_1 + 1) / m_1] \times [(W - r_2 + 1) / m_2]$ tiles. Each tile contains $(m_1 + r_1 - 1) \times (m_2 + r_2 - 1)$ elements, with $r_i - 1$ elements overlapping with neighbouring tiles in each dimension.

The key idea of Winograd convolution is to transform the input tensor and filter tensor from spatial domain into Winograd domain before computation, thereby to reduce the number of multiplications. For instance, the $F(2 \times 2, 3 \times 3)$ configuration achieves a theoretical speedup of 2.25×, $F(4 \times 4, 3 \times 3)$ attains 4× and for $F(6 \times 6, 3 \times 3)$, this value can reach 5.0625×. After computing, the output tensor \hat{O} in Winograd domain will be transformed back. Assume that \hat{i} and \hat{j} are the row and column tile coordinates of the input, so that we have $d = D_{b,c,\hat{i},\hat{j}}$ and $g = F_{k,c}$. The corresponding

output $O_{b,k,\hat{i},\hat{j}}$ can be calculated by Winograd convolution via Equation (3)

$$O_{b,k,\hat{i},\hat{j}} = \sum_{c=1}^C A^T [(GgG^T) \odot (B^T dB)] A = A^T \left[\sum_{c=1}^C [U_{k,c} \odot V_{b,c,\hat{i},\hat{j}}] \right] A, \quad (3)$$

where \odot symbolizes element-wise multiplication, and B, G, A are transformation matrices for input, filter and output respectively. For simplicity, the coordinates (b, \hat{i}, \hat{j}) can be collapsed down to a single dimension ξ . We use (x, y) to denote the coordinates of elements involved in the element-wise multiplication, satisfying $1 \leq x, y \leq m + r - 1$. By performing this transformation, Equation (3) can be converted into its new form as follows:

$$\hat{O}_{k,\xi}^{(x,y)} = \sum_{c=1}^C U_{k,c}^{(x,y)} V_{c,\xi}^{(x,y)}. \quad (4)$$

The progress of Equation (4) can be viewed as matrix multiplication, a Level-3 Basic Linear Algebra Subprograms (BLAS) operation with higher arithmetic intensity compared to element-wise multiplication, which is a Level-1 BLAS operation. The transformation matrices used in Winograd convolution can be generated using the Chinese Remainder Theorem (CRT) [33]. To conserve space, we only provide the input transformation matrices B^T for $F(2 \times 2, 3 \times 3)$ and $F(6 \times 6, 3 \times 3)$ below:

$$B_{2,3}^T = \begin{bmatrix} 1 & 0 & -1 & 0 \\ 0 & 1 & 1 & 0 \\ 0 & -1 & 1 & 0 \\ 0 & -1 & 0 & 1 \end{bmatrix}, \quad B_{6,3}^T = \begin{bmatrix} 1 & 0 & -\frac{21}{4} & 0 & \frac{21}{4} & 0 & -1 & 0 \\ 0 & 1 & 1 & -\frac{17}{4} & \frac{17}{4} & 1 & 1 & 0 \\ 0 & -1 & 1 & \frac{17}{4} & -\frac{17}{4} & -1 & 1 & 0 \\ 0 & -\frac{1}{2} & \frac{1}{4} & -\frac{5}{2} & -\frac{5}{4} & 2 & 1 & 0 \\ 0 & -\frac{1}{2} & \frac{1}{4} & \frac{5}{2} & -\frac{5}{4} & -2 & 1 & 0 \\ 0 & 2 & 4 & -\frac{5}{2} & -5 & \frac{1}{2} & 1 & 0 \\ 0 & -2 & 4 & \frac{5}{2} & -5 & -\frac{1}{2} & 1 & 0 \\ 0 & -1 & 0 & \frac{21}{4} & 0 & -\frac{21}{4} & 0 & 1 \end{bmatrix}. \quad (5)$$

3 SYSTEM DESIGN

We aim to develop a high-performance implementation to accelerate the Winograd convolution process on ARMv8 architectures. Several factors are considered in our approach:

(1) **Cache locality:** Cache has spatial locality and temporal locality. Winograd Convolution has data dependency between its three stages, and processing each stage separately can lead to inefficient use of these cache characteristics.

(2) **Transformation Overhead:** Transforming the Winograd Convolution into GEMM format introduces extra strided memory accesses. Mitigating this overhead and maximizing consecutive memory access while reusing data in vector registers is crucial.

(3) **Matrix Multiplication:** The matrices involved in Winograd Convolution are often irregularly shaped and sometimes small-scale [36, 37]. Performance is significantly influenced by factors such as blocking algorithms, data packing, and edge cases handling. Tailoring designs to these matrices, considering the features of convolution, will be beneficial.

(4) **ARMv8 Architecture-Specific Optimization:** Designing an efficient algorithm for ARMv8 architectures requires careful consideration of register availability and instruction-set characteristics. Selecting an appropriate blocking size—aligned with cache capacity—is critical for maximizing performance. Although using ARM NEON

intrinsic to implement micro-kernels offers convenience and portability, it introduces compiler-dependent optimization behavior, potentially leading to inconsistent performance across different compilers and versions, and it does not allow precise register blocking. By contrast, AArch64 assembly mitigates compiler-related uncertainties and provides more direct access to advanced hardware features that may be inaccessible through intrinsics. This low-level control enables highly optimized instruction pipelines tailored to specific architectural properties, thereby maximizing resource utilization and throughput. However, this approach also entails increased development complexity, as assembly-level programming demands deeper architectural knowledge and greater effort in coding and debugging compared to intrinsics.

(5) **Parallel Strategy:** Convolution layers exhibit diverse scales, making it critical to design multi-dimensional parallel strategies that adaptively determine which dimensions to parallelize based on the problem size, thereby maximizing parallel efficiency.

In consideration of these factors, we employed a variety of optimization techniques. The specifics of our approach will be thoroughly demonstrated in the following subsections. Fig. 1 depicts the overview of our algorithm. Several important notations are used in this figure, including:

- θ : The number of floating-point numbers that can be stored in a vector register. For ARMv8, the bit-width of a vector register is 128 bits, so θ is 4 for FP32 and 2 for FP64.
- L : We assume $L = (m + r - 1) \times (m + r - 1)$, which represents the number of elements in one Winograd tile and the batch size for GEMM.
- T : The number of tiles.
- (α, η) : The parameters of our GEMM micro-kernel. For each computation, it multiplies matrix V with α rows by matrix U with η columns, producing a matrix \hat{O} of shape (α, η) .

In our implementation, we integrated input/filter transformation with data packing operation. The transformed data is stored in z-shape data layout which is optimized for GEMM operations within each block. This design allows the GEMM micro-kernel to access memory consecutively, and ensures that the temporary results of the same C between different blocks of input and filter are also stored consecutively. This arrangement facilitates efficient memory access for subsequent loading. Finally, the T results will be gathered and transformed back into the spatial domain.

Each kernel for the three stages of the Winograd Convolution in our method is implemented using assembly language. This approach allows for precise control over vector registers and enables software prefetching, thereby optimizing the performance and efficiency of our convolution operations. By providing fine-grained control over hardware resources, the use of assembly language ensures that data movement and computation are tightly coupled and efficiently managed, resulting in significant performance improvements.

We propose a fused method for implementing Winograd convolution by integrating the input transformation, GEMM, and output transformation stages. The framework of our method is illustrated in Algorithm 1. In this framework, T_{blk} , C_{blk} and K_{blk} represent the block sizes for tile number, input channels and output channels (also corresponding to the dimensions M, N, K in GEMM), respectively. C_T denotes the number of input channels processed by each input transformation micro-kernel. Unlike the loop order in the algorithm that proposed by GotoBLAS[7], our method requires consideration of not only the loop order and block size for GEMM but also the balance between the transformation and their correlation.

To exploit cache locality, we use two temporary block arrays to store the transformation results of the input and the computation results of GEMM. Filters are entirely transformed into block format with data packing before the main loop

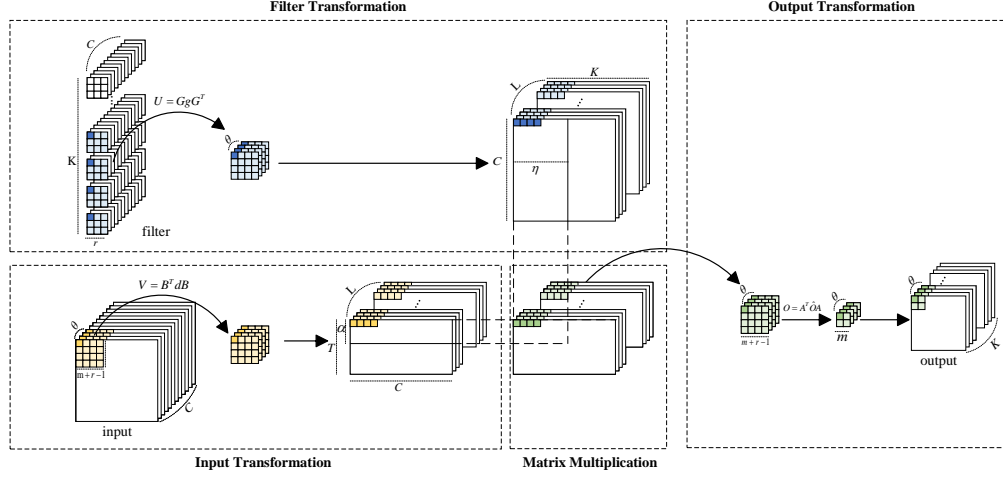


Fig. 1. Overview of the procedure for processing one tile of input using our method, which includes the three stages of Winograd convolution: Input/Filter Transformation, Matrix Multiplication, and Output Transformation. The yellow, blue, and green rectangles represent the data of the input, filter, and output, respectively. The highlighted sections of each color indicate the data loaded into the same vector register, which will be processed simultaneously. After transforming the input and filter, the data is packed into a layout that is friendly to GEMM operations, ensuring consecutive memory access during computation. The results of the GEMM are then transformed back to the spatial domain and stored in the final output.

to avoid repetitive transformations. In inference only mode, filter transformation can be omitted because the weights of the neural network are pre-trained and do not change. Input transformation at line 10 is also designed to avoid repetition. For each iteration at line 14, the GEMM kernel multiplies block matrix $V(T_{blk} \times C_{blk})$ with $U(C_{blk} \times K_{blk})$. Multiple calls to the micro-kernel (α, η) that we mentioned above are integrated into a single assembly kernel to reduce frequent parameter passing between C++ and the general registers when invoking inline assembly. Once the loop over the L dimension is completed, the output transform kernel is executed to transform the corresponding output block and store result.

3.1 Input and filter transformation

As neural networks deepen, the spatial dimensions of the feature maps typically decrease, often due to pooling operations[29], while the number of channels simultaneously increases. This change in dimensions and channel size is a common characteristic of deep neural networks, enabling them to capture more complex features. Table 1 lists the parameters of layers for different mainstream convolutional neural networks. We assume that t_i and t_f respectively denote the number of transform operation for input and filter, where t_i is proportional to $T \times C = \frac{(H-r+1)(W-r+1)C}{m^2} \propto H \times W \times C$ and t_f is proportional to $C \times K$. Given the trends of $H \times W$, C and K as shown in table 1, the transformation time for the input will decrease, while that for the filter will increase. Consequently, these transformations become bottlenecks in different parts of the neural network: the input transformations in the shallower layers and the filter transformations in the deeper layers. Therefore, it is crucial to optimize both input and filter transformations to enhance the overall performance of the Winograd Convolution.

Algorithm 1: Winograd Implementation with GEMM for a single batch

```

Input: Input[C][H][W], Filter[K][C][R][S]
Output: Output[K][P][Q]
// Allocate temporary arrays:
1 TransInOut  $\leftarrow$  new array[ $L \times T_{blk} \times C$ ];
2 GEMMOut  $\leftarrow$  new array[ $L \times T_{blk} \times K_{blk}$ ];
3 FilterOut  $\leftarrow$  new array[ $L \times C \times K$ ];
4 for  $bk = 0$  to  $K$  step  $K_{blk}$  do
5   for  $bc = 0$  to  $C$  step  $C_{blk}$  do
6     Filter Transform Kernel; // Transform the corresponding  $C_{blk} \times K_{blk}$  tiles into the
        Winograd domain with datapacking, and store in
        FilterOut[ $0 : L, bc : bc + C_{blk}, bk : bk + K_{blk}$ ]
7   for  $bt = 0$  to  $T - T\%T_{blk}$  step  $T_{blk}$  do
8     for  $bc = 0$  to  $C$  step  $C_{blk}$  do
9       // Input Transform Kernel
10      for  $ic = 0$  to  $C_{blk}$  step  $C_T$  do
11        Input Transform micro-kernel; // Transform the corresponding  $C_T \times T_{blk}$  tiles into
        the Winograd domain with datapacking, and store in
        TransInOut[ $0 : L, 0 : T_{blk}, bc + ic : bc + ic + C_T$ ]
12      for  $bk = 0$  to  $K$  step  $K_{blk}$  do
13        for  $i = 0$  to  $L$  step 1 do
14          for  $bc = 0$  to  $C$  step  $C_{blk}$  do
15            GEMM Kernel; // Multiply TransInOut[ $i, 0 : T_{blk}, bc : bc + C_{blk}$ ] with
            FilterOut[ $i, bc : bc + C_{blk}, 0 : K_{blk}$ ] and accumulate the result to
            GEMMOut[ $i, 0 : T_{blk}, 0 : K_{blk}$ ]
16          Output Transform Kernel; // Transform GEMMOut[ $0 : L, 0 : T_{blk}, bk : bk + K_{blk}$ ] back to the
            spatial domain and store in Output
16 Process the remaining  $T\%T_{blk}$  tiles. The framework follows the same procedure as described above, but with
    kernels utilizing different values of  $\alpha$  and  $\eta$ .

```

3.1.1 Transformation. We implemented three widely used Winograd Convolution variants ($m = 2$, $m = 4$ and $m = 6$), and adopt two distinct transformation strategies based on the $F(m \times m, r \times r)$ configuration. Specifically, for $F(2 \times 2, 3 \times 3)$, where the architecture supports at least $2L$ vector registers, we employ a different approach than for $F(4 \times 4, 3 \times 3)$ and $F(6 \times 6, 3 \times 3)$, which operate under fewer than $2L$ vector registers. Because the latter two variants share the same processing logic, we use share the same logic, we use $F(6 \times 6, 3 \times 3)$ as an illustrative example. The transformation matrices employed in our method are provided by `wincnn` [18]. However, for both methods, each vector register contains θ values from the same coordinates (x, y) within a tile, as mentioned in Equation (4), but across θ channels. Since the transformation processes for the input and the filter are generally similar, we will primarily focus on the details of the input transformation in the following text.

F(2×2, 3×3): the ARMv8 processor has 32 128-bit vector registers. For this scale, each tile contains $4 \times 4 = 16$ elements, allowing 16 inputs and 16 transformed results across $\theta = 4$ channels to be held in the vector registers simultaneously. Because the Winograd Convolution employs the OLA method, and the data are stored in row-major order, adjacent tiles in the W dimension share 8 elements, enabling register reuse. The processing order of the input is $W \rightarrow H \rightarrow C$. Therefore, we only need to load all 16 elements during the initial pass in the W direction. For subsequent tiles, only 8 elements per tile need to be loaded. This approach can nearly halve the number of load instructions required. Some

details are depicted in Fig. 2, where each number represents the index of a vector register. Another advantage of this arrangement is that we can omit the elements that are zero in the transformation matrix $B_{2,3}$ as shown in Equation (5), and for elements with a value of 1, we only need to perform addition and subtraction operations. This significantly reduces the number of calculation operations required.

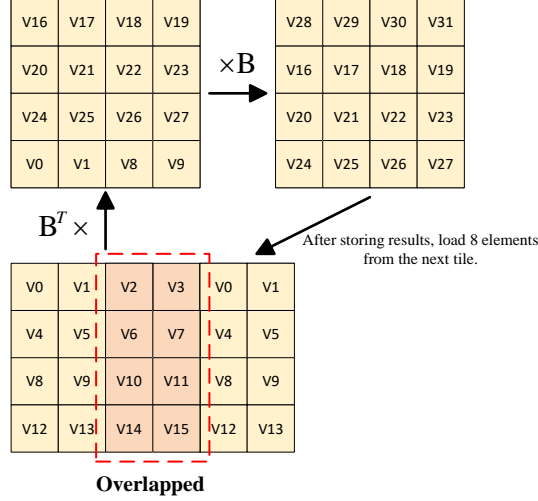


Fig. 2. This figure illustrates the transformation process of $F(2 \times 2, 3 \times 3)$. Each vector register contains θ elements. For simplicity, we present a front view of this process. The figure demonstrates the register arrangement of our method, with numbers denoting the index of the vector registers. In the initial iteration, the entire tile is loaded into registers v_0 to v_{15} , while v_{16} to v_{31} are used to store the results. When left-multiplying with B^T , registers v_0, v_1, v_8 and v_9 are freed to store the temporary results. After processing the first tile, data in registers $v_2, v_3, v_6, v_7, v_{10}, v_{11}, v_{14}$ and v_{15} can be reused, requiring only the non-overlapping data of the second tile to be loaded into $v_0, v_1, v_4, v_5, v_8, v_9, v_{12}$ and v_{13} . For the next tile, the process is reversed: reusing $v_0, v_1, v_4, v_5, v_8, v_9, v_{12}$ and v_{13} , and loading new data into $v_2, v_3, v_6, v_7, v_{10}, v_{11}, v_{14}$ and v_{15} . This alternating pattern continues for subsequent iterations, significantly reducing the number of elements that need to be loaded.

$F(6 \times 6, 3 \times 3)$: For this scale, each tile contains $8 \times 8 = 64$ elements, which exceeds the number of vector registers. Consequently, we have to process only part of a tile at a time. Our design is to process one row (8 elements) per iteration. To fully utilize the vector registers, we hold elements across 2θ channels simultaneously. Since the data are stored in row-major order, we first perform the multiplication $d \times B$ and then store the temporary result tmp in a temporary array of size $8 \times 8 \times 8$. Subsequently, we left-multiply this tensor with B^T . By leveraging the special structure of $B_{6,3}$ we can extract common computational factors, thereby reducing the overall computational complexity. The computation for the i -th row can be carried out as shown in Equation (6), which is equivalent to the left multiplication by the $i - th$

column of $B_{6,3}^T$,

$$\begin{aligned}
 f_0 &= d^{(i,3)} + d^{(i,7)} - 4.25 \times d^{(i,4)}, \\
 f_1 &= d^{(i,2)} - 4.25 \times d^{(i,4)} + d^{(i,6)}, \\
 f_2 &= 1.25 \times d^{(i,5)}, \\
 f_3 &= 2.5 \times d^{(i,4)}, \\
 f_4 &= 0.25 \times d^{(i,3)} - f_2 + d^{(i,7)}, \\
 f_5 &= 0.5 \times d^{(i,2)} - f_3 + 2 \times d^{(i,6)}, \\
 f_6 &= 4 \times (d^{(i,3)} - f_2) + d^{(i,7)}, \\
 f_7 &= 2 \times d^{(i,2)} - f_3 + 0.5 \times d^{(i,6)},
 \end{aligned}
 \quad
 tmp^{iT} = \begin{bmatrix}
 d^{(i,1)} + 5.25 \times (d^{(i,5)} - d^{(i,3)}) - d^{(i,7)} \\
 f_0 + f_1 \\
 f_0 - f_1 \\
 f_4 + f_5 \\
 f_4 - f_5 \\
 f_6 + f_7 \\
 f_6 - f_7 \\
 5.25 \times (d^{(i,4)} - d^{(i,6)}) - d^{(i,2)} + d^{(i,8)}
 \end{bmatrix}. \quad (6)$$

The filter transformation, unlike input transformation, involves spatially loading data across the C and K dimensions in the spatial domain. However, following the GEMM-friendly data layout designed in the Winograd domain, η (i.e., K) represents the fastest-varying direction. If data loaded into the same vector register spans θ channels along the C dimension, although it ensures fully consecutive memory access in the spatial domain, storing transformation results will span dimensions L and C, which causes each storage instruction to accommodate only one datum, thus nullifying the advantage of vector registers. To achieve contiguous memory access when loading data and to maximize partial continuity in the Winograd domain, thereby reducing storage instruction usage, the filter transformation loads θ channels from the K dimension into vector registers and processes them in the order of $\theta \rightarrow C \rightarrow \frac{K}{\theta}$.

3.1.2 Data packing. In order to ensure consecutive memory access for Matrix Multiplication, we store the transformed results in GEMM friendly format. The data layout of *TransInOut* and *FilterOut* are $[L][C/C_{blk}][T_{blk}/\alpha][C_{blk}/\theta][\alpha][\theta]$ and $[K/K_{blk}][L][C/C_{blk}][K_{blk}/\eta][C_{blk}][\eta]$ as showed in Fig. 3(a) and Fig. 3(b), respectively. Here, η is a multiple of θ for vectorization load. Since the memory access for spatial input spans the C dimension and the transformed results are scattered across L different memory blocks, ensuring consecutive memory access is challenging. Our goal is to mitigate this issue. For $F(2 \times 2, 3 \times 3)$, we reduce the number of load instructions by first looping in the W direction, as previously mentioned. For $F(6 \times 6, 3 \times 3)$, the processing order of our approach is $C \rightarrow W \rightarrow H$, ensuring consecutive memory access within each coordinate (x, y) corresponding memory area.

3.2 Matrix Multiplication

We employ micro-kernels to process GEMM, each of which computes α rows of the blocked transformed input matrix with η columns of the blocked transformed filter matrix. This approach represents a key optimization in our method. We do not solely focus on achieving a high computation-to-memory ratio (CMR); we also consider other critical factors such as pipeline bubbles, edge cases, and the optimal block sizes for the matrices. These considerations collectively contribute to enhancing the efficiency and robustness of our implementation.

3.2.1 micro-kernel design. As illustrated in Fig. 3, the data layout of the transformed input and filter requires α , $\eta/4$, $\alpha \times \eta/4$ vector registers to load and store the input, filter, and output, respectively, for FP32 precision. To avoid pipeline bubbles and maintain sufficient interleaving between the load and compute operations, we employ the "ping-pong" technique [32]. This technique necessitates additional α and $\eta/4$ registers to load data for the next iteration. Consequently, the number of vector registers required must satisfy the following condition:

$$2\alpha + \eta/2 + \alpha \times \eta/4 \leq 32. \quad (7)$$

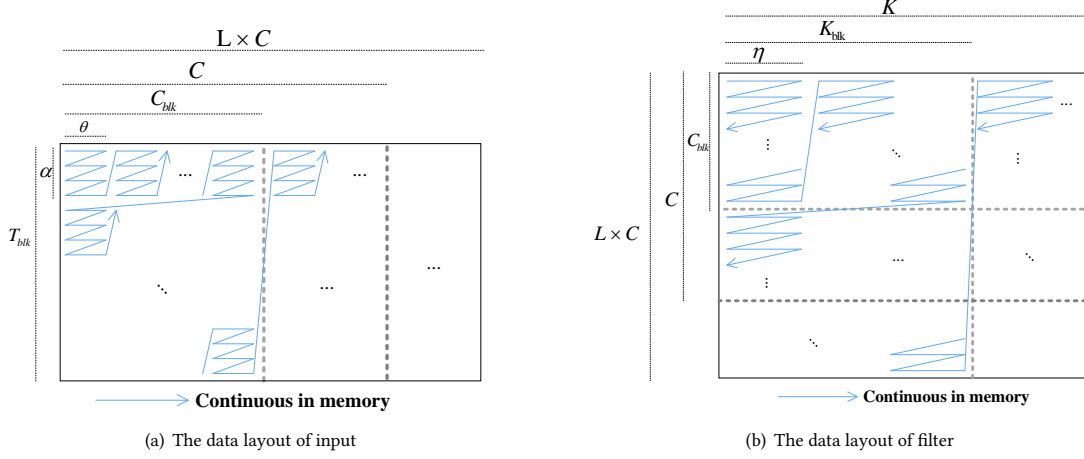


Fig. 3. This figure depicts the data layout used in our implementation for the transformed input and filter. The core concept of our method is to initially divide the original matrix into blocks that fit within the cache capacity. These blocks are then processed using multiple micro-kernels for GEMM operations. Each micro-kernel handles the matrix multiplication involving α rows and η columns. By organizing the data layout in this manner, we ensure continuous memory access, which significantly improves performance. In this figure, we primarily highlight the data arrangement within each block and the relationships between blocks.

We set η to satisfy the constraint described in Equation (8) to accommodate SIMD loading for FP32 precision. In convolutional networks, the filter dimension K is invariably a multiple of 16. Consequently, we configure the block size of K to also be a multiple of 16. This deliberate selection, as elaborated in Subsection 3.2.2, mitigates potential edge cases in the K dimension, which could otherwise diminish the Arithmetic Intensity (AI) of the microkernel:

$$\eta \% 4 = 0. \quad (8)$$

Achieving a high CMR is a primary optimization objective in our approach. For θ iterations, our methodology necessitates α load instructions for the input and $[(\eta/\theta) \times \theta]$ load instructions for the filter. Additionally, it requires $\alpha \times \eta$ scalar-vector FMA instructions, each encompassing two operations. Therefore, the average CMR of our method can be computed as follows:

$$\frac{2 \times \alpha \times \eta}{\alpha + \eta}. \quad (9)$$

Our objective can be articulated as a constrained optimization problem aimed at maximizing Equation (9) under the constraints delineated in Equations (7) and (8). Through this formulation, we derive the optimal parameters as $\alpha = 7$ and $\eta = 8$. Additionally, as demonstrated in Table 1, the observed trends in input and filter dimensions suggest that the dimension T will decrease while dimensions C and K will increase. This implies that edge cases in the T dimension will become progressively more time-consuming. To mitigate this, we have also implemented a sub-optimal micro-kernel with parameters $\alpha = 4$ and $\eta = 16$, which reduces the number of edge cases in the T dimension. Our strategy involves transitioning from the (7, 8) micro-kernel to the (4, 16) micro-kernel as C and K surpass T in magnitude.

The vector register arrangement for the micro-kernel is depicted in Fig. 4. In the (4,16) configuration, we employ registers $v0$ to $v3$ and $v4$ to $v7$ as two sets of registers for loading the input, while registers $v8$ to $v11$ and $v12$ to $v15$ are utilized for loading the filter. Registers $v16$ to $v31$ are designated for storing the corresponding results. Owing to

the scalar-vector FMA operation, each set of input registers is released after four pipeline stages, whereas the filter registers are released at each stage, as illustrated in Fig. 4(a).

Initially, the entire 4×4 elements are loaded into the first set of input registers, and 16×2 elements are loaded into the two sets of filter registers to launch the process. At each subsequent pipeline stage, our approach prefetches 4 elements into one SIMD register of another set of input registers and 16 elements into another set of filter registers. This method ensures adequate interleaving between load and compute instructions for the same data, allowing the computation of the final stage to overlap with the loading for the next stage.

The process for the (7,8) micro-kernel configuration is analogous to that of the (4,16) configuration. However, in the (7,8) configuration, the prefetched elements for the input are 8 for the first three stages of each four-stage group and 4 for the last stage. This detailed register configuration for the (7,8) micro-kernel is shown in Fig. 4(b).

This strategic arrangement and interleaving ensure optimal use of the vector registers, minimizing idle times and maximizing computational efficiency. The design is carefully crafted to balance the load and computation phases, enhancing the overall performance of the micro-kernel.

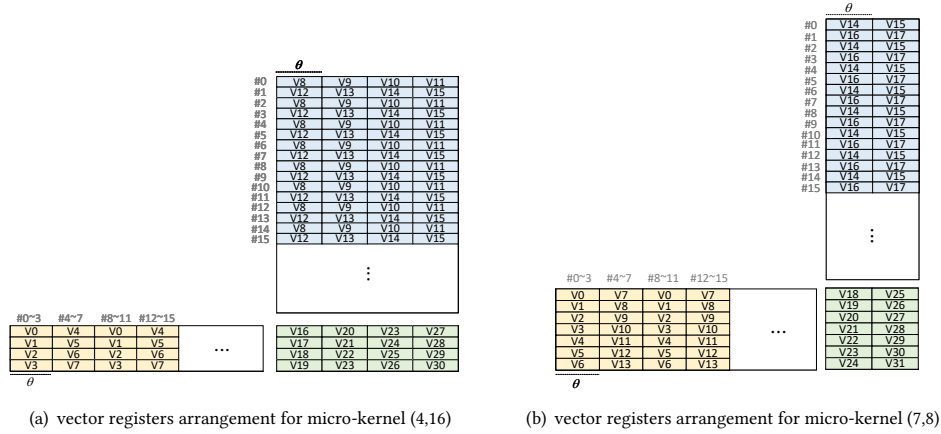


Fig. 4. This figure illustrates the arrangement of vector registers for the micro-kernel. The notation $\#num$ denotes the stage number of the pipeline in the "ping-pong" technique, and each number represents the index of the vector register. Both configurations utilize the entire set of 32 SIMD registers. The yellow, blue, and green rectangles represent the data of the input, filter, and result, respectively.

3.2.2 Blocking sizes analysis. Our approach employs a heuristic-based method to determine the blocking size during the instantiation phase, with a design principle grounded in the cache capacity to minimize data movement overhead. This strategy ensures that the blocks are appropriately sized to optimize performance. During the iteration in the C direction, as outlined in line 13 of Algorithm 1, the $T_{blk} \times K_{blk}$ block of output should be consistently retained in the L2 cache. Additionally, the L2 cache must accommodate the $T_{blk} \times C_{blk}$ block of input and the $C_{blk} \times K_{blk}$ block of filter for the current iteration. Moreover, it should prefetch the necessary blocks for the subsequent iteration.

We denote the cache capacity as \mathbb{C} . Thus, the blocking parameters must be carefully chosen to satisfy the following constraint:

$$T_{blk} \times K_{blk} + 2 \times (T_{blk} \times C_{blk} + C_{blk} \times K_{blk}) < \mathbb{C}_{L2}. \quad (10)$$

In GEMM kernel, our design prioritizes the processing of T_{blk}/α blocks of size $\alpha \times C_{blk}$ for the input, utilizing the same $C_{blk} \times \eta$ block of the filter for the micro-kernel. Furthermore, the corresponding $T_{blk} \times K_{blk}$ block of results is retained in the L1 cache.

To ensure that the L1 cache can accommodate the necessary data blocks, the capacity constraint is given by

$$T_{blk} \times K_{blk} + 2 \times \alpha \times C_{blk} + C_{blk} \times \eta < \mathbb{C}_{L1}. \quad (11)$$

We use \mathbb{B} to denote the data transfer bandwidth of each level of the memory hierarchy, where \mathbb{B}_M represents the data transfer bandwidth of the levels below the L2 cache (i.e., Last Level Cache (LLC) and main memory). Thus, the total data movement overhead for input, filter, and output can be modeled as follows:

$$\begin{aligned} \mathbb{O}_{input} &\approx \frac{T}{T_{blk}} \times \frac{K}{K_{blk}} \times L \times \frac{C}{C_{blk}} \times \left[\left(\frac{T_{blk}}{\alpha} \times \frac{K_{blk}}{\eta} \times \alpha \times C_{blk} \right) \times \left(\frac{1}{\mathbb{B}_{L1}} + \frac{1}{\mathbb{B}_{L2}} \right) + \frac{T_{blk} \times C_{blk}}{\mathbb{B}_M} \right] \\ &= \frac{T \times K \times L \times C}{\eta} \times \left(\frac{1}{\mathbb{B}_{L1}} + \frac{1}{\mathbb{B}_{L2}} \right) + \frac{T \times K \times L \times C}{K_{blk} \times \mathbb{B}_M}, \end{aligned} \quad (12)$$

$$\begin{aligned} \mathbb{O}_{filter} &\approx \frac{T}{T_{blk}} \times \frac{K}{K_{blk}} \times L \times \frac{C}{C_{blk}} \times \left[\left(\frac{K_{blk}}{\eta} \times C_{blk} \times \eta \right) \times \left(\frac{1}{\mathbb{B}_{L1}} + \frac{1}{\mathbb{B}_{L2}} \right) + \frac{C_{blk} \times K_{blk}}{\mathbb{B}_M} \right] \\ &= \frac{T \times K \times L \times C}{T_{blk}} \times \left(\frac{1}{\mathbb{B}_{L1}} + \frac{1}{\mathbb{B}_{L2}} + \frac{1}{\mathbb{B}_M} \right), \end{aligned} \quad (13)$$

$$\begin{aligned} \mathbb{O}_{output} &\approx \frac{T}{T_{blk}} \times \frac{K}{K_{blk}} \times L \times \left[T_{blk} \times K_{blk} \times \left(\frac{1}{\mathbb{B}_{L2}} + \frac{1}{\mathbb{B}_M} \right) + \frac{C}{C_{blk}} \times \frac{T_{blk}}{\alpha} \times \frac{K_{blk}}{\eta} \times \frac{\alpha \times \eta}{\mathbb{B}_{L1}} \right] \\ &= T \times K \times L \times \left[\left(\frac{1}{\mathbb{B}_{L2}} + \frac{1}{\mathbb{B}_M} \right) + \frac{C}{C_{blk} \times \mathbb{B}_{L1}} \right]. \end{aligned} \quad (14)$$

Therefore, we can calculate the total data movement overhead \mathbb{O} by summarizing Equations (12), (13) and (14) into the following expression:

$$\begin{aligned} \mathbb{O} &= \mathbb{O}_{input} + \mathbb{O}_{filter} + \mathbb{O}_{output} \\ &= T \times K \times L \times C \times \left[\left(\frac{1}{\eta} + \frac{1}{T_{blk}} + \frac{1}{C_{blk}} \right) \times \frac{1}{\mathbb{B}_{L1}} + \left(\frac{1}{\eta} + \frac{1}{T_{blk}} + \frac{1}{C} \right) \times \frac{1}{\mathbb{B}_{L2}} + \left(\frac{1}{\eta \times K_{blk}} + \frac{1}{T_{blk}} + \frac{1}{C} \right) \times \frac{1}{\mathbb{B}_M} \right]. \end{aligned} \quad (15)$$

The strategy of our method focuses on minimizing Equation (15) under the constraints specified in Equations (10) and (11). Considering the characteristics of the channels in convolutional neural networks, both K_{blk} and C_{blk} are configured to be divisible by 16. This configuration ensures that η satisfies Equation (8), thereby circumventing potential edge cases that could arise in the K and C dimension. By setting K_{blk} and C_{blk} to be multiples of 16, we can streamline the computational process, enhancing both the efficiency and stability of the GEMM operation.

3.3 Output Transformation

After executing computations in the Winograd domain, the results need to be transformed back into the spatial domain. The number of inverse transform operations t_o is proportional to $T \times K$, which decreases as the convolutional network deepens. This procedure in our approach is analogous to the input and filter transformations demonstrated in Subsection 3.1, where each SIMD register holds θ elements simultaneously. To exploit cache locality, the output transformation kernel is invoked as soon as the computation of the results $L \times T_{blk} \times K_{blk}$ is complete, when these results are stored in a temporary array, as outlined in Algorithm 1. The data layout of this temporary array is structured as $[L][K_{blk}/\eta][T_{blk}/\alpha][\eta/\theta][\alpha][\theta]$, which ensures continuous memory access for GEMM storage and facilitates efficient

loading during the inverse transformation. Subsequently, the results in the spatial domain are stored back into the main memory following the standard convolutional neural network format $[N][K][P][Q]$.

3.4 Parallel Strategies

We employed OpenMP [3] to parallelize the fused method framework presented in Algorithm 1, utilizing static scheduling to pre-allocate workloads to each available core/thread.

The primary objective is to achieve a balanced distribution of the computational workload across threads for convolution layers of varying sizes, thereby reducing core idling, minimizing cache contention and synchronization overhead, with the aim of enhancing parallel efficiency and scalability.

To fully exploit the ARM architecture and achieve these goals, we adopted a multi-dimensional parallelization strategy which combines inter-batch and intra-batch parallelization. Specifically, we parallelized the loops corresponding to dimensions in lines 7, 8, 9, and 11 of Algorithm 1, as well as the outermost batch dimension. The dimensions involved in parallelization include N , T and C/K , which together form a three-level parallelism structure. Correspondingly, the available P threads are divided into a three-dimensional grid of $P_N \times P_T \times P_{C/K}$. By collapsing lines 8 and 9 of Algorithm 1 along the C dimension, the total number of sub-tasks is the product of the sub-task counts in the N , T , and C - K dimensions, given by $N \times \frac{T}{T_{blk}} \times \left(\frac{C}{C_T} + \frac{K}{K_{blk}} \right)$. To ensure that each thread has sufficient work and that the number of sub-tasks is as evenly divisible by the number of threads as possible, the maximum thread counts for the N , T , and C/K dimensions are empirically set to $\max(1, N/2)$, $\max(1, 2^{\lceil \log_2 \left(\frac{T/T_{blk}}{4} \right) \rceil})$, and $\max\left(\frac{\min(C/C_T, K/K_{blk})}{4}, 1\right)$, respectively. For convenience, these values will be referred to as P_N^{max} , P_T^{max} , and $P_{C/K}^{max}$ in subsequent discussions.

Given the aim of maximizing the independence of sub-tasks executed within the same thread/core, the parallelism priority is set as $\mathcal{P}(N) > \mathcal{P}(T) > \mathcal{P}(C/K)$, where $\mathcal{P}(X)$ denotes the priority of dimension X . Therefore, the thread allocation across dimensions in the thread grid can be recursively determined as $P_N = \min(P, P_N^{max})$, $P_T = \min(P/P_N, P_T^{max})$, and $P_{C/K} = P/(P_N \times P_T)$. When $P \leq P_N^{max}$, only inter-batch parallelism is performed; otherwise, intra-batch parallelism is enabled simultaneously. Intra-batch parallelism can be further categorized into three modes based on problem size: the T mode for layers with a sufficient number of tiles to offer adequate parallelism, the multi-dimensional mode when the thread count exceeds the maximum number of threads in the T -dimension, and the C/K mode for layers where T is relatively small and not worth parallelizing, with T_{blk} set to T .

We implement static workload distribution within a single parallel region to mitigate overhead due to thread allocation and destruction in the inner loops introduced by OpenMP nested parallelism. The C/C_T sub-tasks of the input transformation and the K/K_{blk} sub-tasks of the fused GEMM and output transformation are executed in parallel by unit thread groups, each consisting of $P_{C/K}$ threads. P_T unit thread groups form a composite group ($P_T \times P_{C/K}$ threads) to perform intra-batch parallelization. Likewise, P_N composite groups enable parallelism along batches. Synchronization within the unit thread group is required after input transformation. We employed an intra-group synchronization mechanism based on sense variables and OpenMP atomic operations to enhance the efficiency while ensuring its correctness.

4 EXPERIMENTS

In this section, we present a comprehensive performance and accuracy evaluation of our proposed method relative to NCNN [30], NNPACK [5], FastConv [22], and the ACL [6]. As summarized in Table 1, we benchmark the widely adopted VGG-16 [26] and FusionNet [23], which together represent a range of network scales. The experiments were

conducted on three distinct ARMv8-based platforms. Specifically, we employed (1) a Kunpeng 920 processor [10] with 64 KB L1 instruction/data caches, a 512 KB L2 cache, and a 64 MB shared L3 cache; (2) an AWS Graviton2 M6g instance [25] with 64 KB L1 instruction/data caches, a 1 MB L2 cache, and a 32 MB shared L3 cache; and (3) a Phytium 2000+ processor [27] with 64 KB L1 instruction/data caches and a 2 MB L2 cache shared by a four-core cluster, but no L3 cache. These results demonstrate the feasibility and efficacy of our Winograd convolution optimization strategy, highlighting its potential for achieving superior performance on a broad range of ARMv8 architectures.

NCNN dynamically selects among three Winograd convolution variants— $F(2 \times 2, 3 \times 3)$, $F(4 \times 4, 3 \times 3)$, and $F(6 \times 6, 3 \times 3)$ —based on the problem scale, and implements these configurations using GEMM. NNPack adopts only the $F(6 \times 6, 3 \times 3)$ configuration with Tuple Element-Wise Multiplication (TEWMM), which exhibits lower arithmetic intensity than GEMM while significantly reducing transformation overhead. FastConv, a high-performance library optimized for ARM CPUs, implements $F(6 \times 6, 3 \times 3)$ Winograd convolution through TensorGEMM, a GEMM-like algorithm. Although TensorGEMM shares a similar arithmetic intensity expression with GEMM, under the same vector register constraints it demonstrates lower arithmetic intensity, and similarly mitigates transformation costs. Finally, the ACL employs a $F(4 \times 4, 3 \times 3)$ Winograd convolution with GEMM and introduces additional data packing operations following the transformation step.

Table 1. Different convolution neural networks.

Layer	C	K	H & W	R & S
VggNet_1.2	64	64	224	3
VggNet_2.2	128	128	112	3
VggNet_3.2	256	256	56	3
VggNet_4.2	512	512	28	3
VggNet_5.2	512	512	14	3
FusionNet_1.2	64	64	640	3
FusionNet_2.2	128	128	320	3
FusionNet_3.2	256	256	160	3
FusionNet_4.2	512	512	80	3
FusionNet_5.2	1024	1024	40	3

4.1 Single-core Performance Evaluation

To assess the optimization efficiency of each $F(m, r)$ configuration, we conducted a stepwise evaluation comparing our approach against alternative libraries, each evaluated using its corresponding $F(m, r)$ variant on the Kunpeng920. For NCNN, we manually disabled its dynamic selection mechanism to ensure a fair baseline. The results, presented in Figure 5, indicate that our method consistently outperforms the other libraries on a single-core basis for every layer of the chosen benchmark networks.

Specifically, relative to NCNN, our approach achieves up to 2.08 \times , 2.83 \times , and 3.84 \times speedups for $F(2 \times 2, 3 \times 3)$, $F(4 \times 4, 3 \times 3)$, and $F(6 \times 6, 3 \times 3)$, respectively. Compared to ACL, NNPack, and FastConv—with each employing its respective $F(m, r)$ variant—our method yields speedups ranging from 1.11 \times to 3.09 \times , 1.58 \times to 1.84 \times , and 1.38 \times to 2.21 \times , respectively.

Furthermore, we evaluated the computational efficiency of our approach in GFlop/s on the Kunpeng 920, comparing it against NCNN, NNPack, FastConv, and ACL under identical $F(m, r)$ configurations (see Fig.6). As discussed in

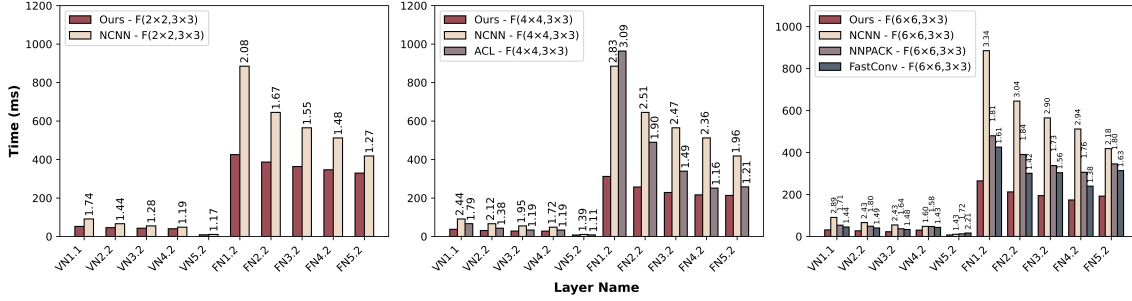


Fig. 5. Step-wise comparison of the convolution layers’ runtime against NCNN, NNPack, FastConv and ACL with the same $F(m, r)$ on the Kunpeng920. Each point on the x-axis represents a different layer, with VN and FN being abbreviations for VggNet and FusionNet, respectively. The y-axis denotes the runtime in milliseconds (*ms*). The left figure shows $F(2 \times 2, 3 \times 3)$, the middle figure shows $F(4 \times 4, 3 \times 3)$ and the right figure shows $F(6 \times 6, 3 \times 3)$. Each number above the bars represents the speedup our approach achieves compared to the corresponding library.

Equation(15), increasing L (where $L = 16$ for $F(2 \times 2, 3 \times 3)$, $L = 36$ for $F(4 \times 4, 3 \times 3)$, and $L = 64$ for $F(6 \times 6, 3 \times 3)$) intensifies data movement overhead. This escalation leads to a downward trend in computational efficiency as m increases when employing our GEMM-based implementation.

For smaller layers, such as VggNet5.2, a pronounced decrease in GFlop/s is observed. This is attributed to the limited computational load, resulting in a low compute-to-memory ratio (CMR). Consequently, as m increases, these layers become memory-bound—particularly in the $F(6 \times 6, 3 \times 3)$ case—thereby restricting full hardware utilization.

NNPACK relies on TEWMM, a Level-1 BLAS operation, which inherently provides lower computational efficiency than GEMM-based routines (Level-3 BLAS), since Level-3 BLAS operations more effectively amortize memory access costs. Although TensorGEMM (employed by FastConv) outperforms TEWMM, it still exhibits suboptimal performance compared to libraries leveraging GEMM operations.

In comparison, our method consistently surpasses NCNN and ACL, both of which are GEMM-based, and demonstrates progressively stronger performance as the computational workload increases. Notably, our approach attains up to 94.81% of the Kunpeng 920’s single core theoretical peak performance for $F(2 \times 2, 3 \times 3)$ in layer FN2.2. Moreover, for most benchmarked layers, our GEMM routines maintain efficiencies exceeding 90% of the single processor theoretical peak performance.

Next, we conducted a step-wise evaluation of our approach compared to other libraries across all benchmark layers, as illustrated in Fig. 7. Our method employs a heuristic algorithm to determine the appropriate $F(m, r)$ configuration based on network scale, similar to NCNN, and this selection process is performed at the initialization stage, thereby incurring no additional runtime overhead. All other libraries were evaluated with their default settings.

On the Kunpeng 920 (single-core), our method achieves speedups of 1.13x to 1.81x over NCNN, 1.61x to 1.84x over NNPack, 1.37x to 2.21x over FastConv, and 1.41x to 3.63x over ACL. On the AWS Graviton2 platform (single-core), the observed speedups range from 1.08x to 1.54x against NCNN, 1.25x to 1.58x against NNPack, 1.35x to 5.52x against FastConv, and 1.10x to 1.86x against ACL. Similarly, on the Phytium 2000+ (single-core), our approach outperforms NCNN, NNPack, FastConv, and ACL by 1.08x to 1.54x, 1.25x to 1.58x, 1.35x to 5.52x, and 1.10x to 1.86x, respectively.

To validate the effectiveness of our fused framework, we measured the Last Level Cache (LLC) miss rates on the Kunpeng 920, as illustrated in Fig. 8, and compared our results against those of other libraries. Across most benchmark

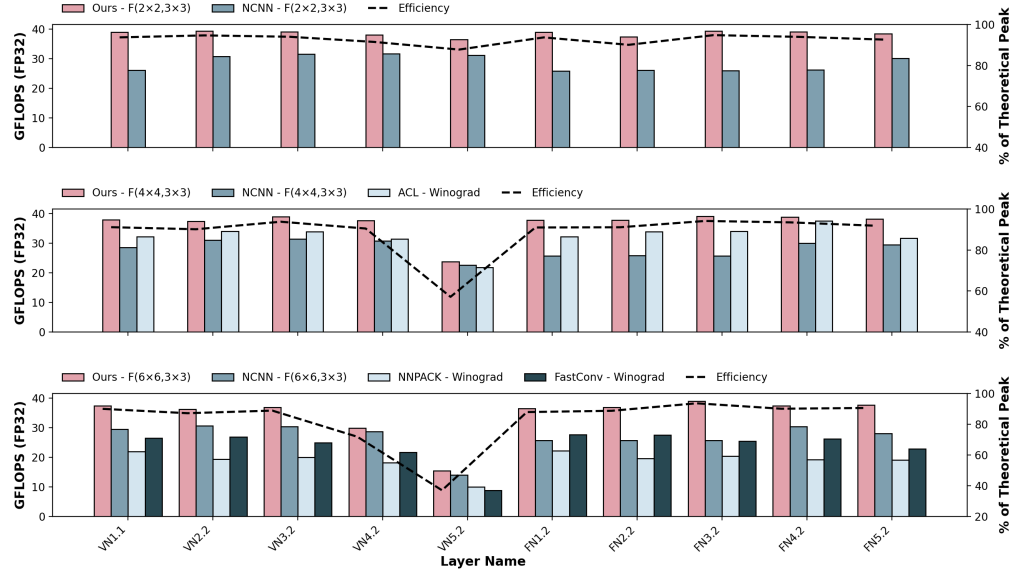


Fig. 6. Layer-wise evaluations of the computational performance against NCNN, NNPack, FastConv and ACL with the same $F(m, r)$. In the figure, the left y-axis represents performance in GFlop/s, while the right y-axis indicates the fraction of the theoretical single-core peak performance (41.6 GFlop/s) on the Kunpeng 920. For VggNet5.2, the small problem scale results in a memory-bound scenario, leading to decreased GFlop/s for $F(4 \times 4, 3 \times 3)$ and $F(6 \times 6, 3 \times 3)$.

layers, our method consistently achieves lower LLC miss rates, demonstrating more efficient cache utilization. The sole exception is the FN5.2 layer, where the large values of K and C result in an extensive filter data footprint. This increased data volume causes frequent cache replacements and heightens cache pressure, ultimately reducing performance gains for that particular layer.

4.2 Multi-cores Convolution

For multi-core performance evaluations using 8 and 16 threads on the Kunpeng 920, AWS Graviton2, and Phytium 2000+ platforms (Fig. 7), our approach demonstrates superior scalability and consistently outperforms NCNN, NNPack, FastConv, and ACL.

Average speedups:

- **Kunpeng 920:** With 8 threads, our method achieves mean speedups of 2.05 \times , 2.27 \times , 3.01 \times , and 1.95 \times over NCNN, NNPack, FastConv, and ACL, respectively. With 16 threads, these speedups increase to 2.07 \times , 2.18 \times , 3.78 \times , and 2.07 \times .
- **AWS Graviton2:** At 8 threads, the corresponding speedups are 1.54 \times , 1.34 \times , 2.97 \times , and 2.31 \times , rising to 1.94 \times , 1.60 \times , 4.32 \times , and 2.86 \times at 16 threads.
- **Phytium 2000+:** our approach outperforms NCNN, NNPack, FastConv, and ACL by factors of 1.79 \times , 2.00 \times , 3.36 \times , and 4.01 \times , and 2.31 \times , respectively. Increasing to 16 threads yields improvements of 1.93 \times , 1.76 \times , 4.14 \times , and 4.13 \times .

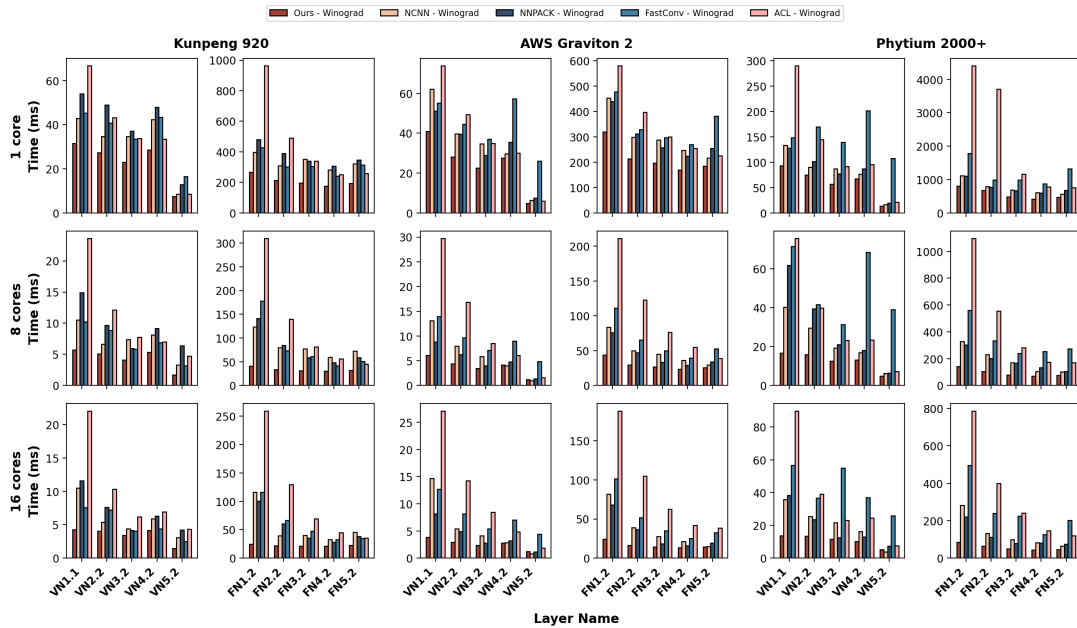


Fig. 7. Step-wise comparison of convolution layer runtimes (single-core, 8-core, and 16-core) against NCNN, NNPACK, FastConv, and ACL on the Kungpeng 920, AWS Graviton2, and Phytium 2000+ platforms.

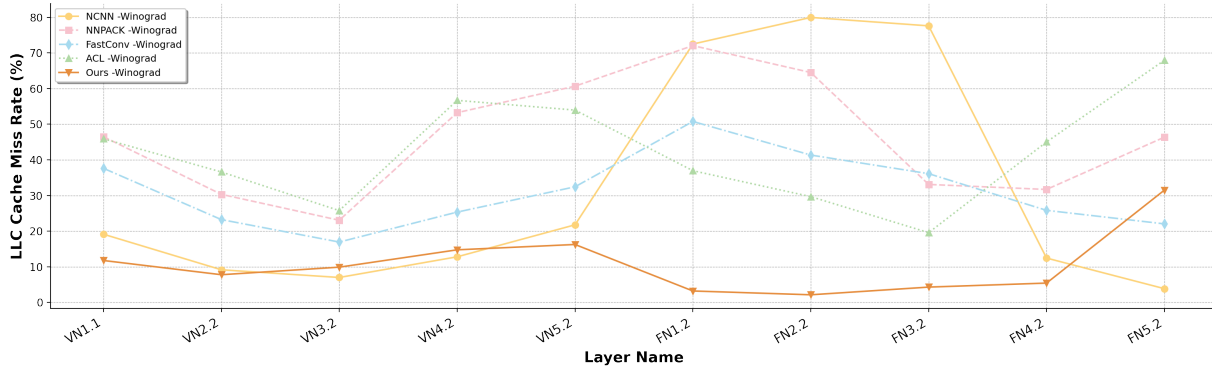


Fig. 8. LLC cache miss rates compared to other libraries on the Kungpeng920.

Maximum speedups:

- **Kungpeng 920:** Up to 3.00×, 3.81×, 4.33×, and 7.54× with 8 threads, and 4.74×, 4.10×, 4.72×, and 10.57× with 16 threads over NCNN, NNPACK, FastConv, and ACL, respectively.
- **AWS Graviton2:** Maximum gains reach 2.16×, 1.73×, 4.10×, and 4.91× with 8 threads, and 3.85×, 2.81×, 4.20×, and 7.80× with 16 threads.
- **Phytium 2000+:** We observe speedups of up to 2.40×, 3.68×, 8.00×, and 7.80× with 8 threads, and 3.32×, 2.78×, 5.84×, and 9.28× with 16 threads.

These results underscore the scalability and robust performance of our approach across diverse platforms and threading configurations. While our fused framework complicates precise computation efficiency measurements under multi-threaded conditions, we nevertheless evaluated the parallel execution efficiency of our method and other libraries using 8 and 16 threads, as shown in Fig. 9. Our approach consistently achieves higher parallel efficiency across all benchmark layers, particularly in those with larger problem sizes and greater floating-point workloads, thereby surpassing the parallelization quality of competing libraries. The VN5.2 layer represents an exception, as its relatively small problem size does not allow sufficient task decomposition to fully exploit parallel execution.

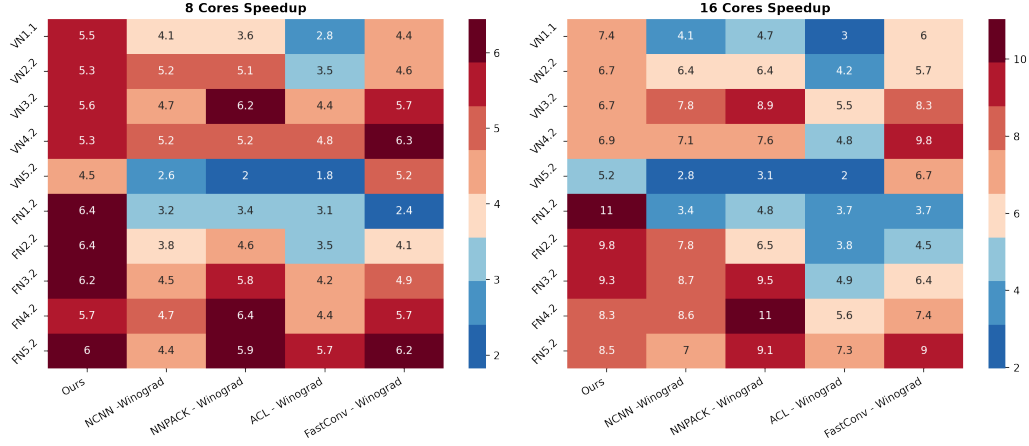


Fig. 9. Layer-wise evaluations of the speedup of parallel execution against single-thread execution.

4.3 Accuracy

Table 2 reports the average and maximum errors across all layers of our implementation, as well as a comparison with other libraries. The results use single-precision floating-point direct convolution as the reference baseline, with inputs and filters drawn from a uniform distribution within $[-1.0, 1.0]$. As shown, error magnitudes increase alongside larger m values, reflecting the heightened sensitivity introduced by the transform matrices in Winograd Convolution [19].

Despite this trend, convolutional neural networks typically tolerate low-precision computations, and errors below 10^{-2} have been reported to leave training and inference stability largely unaffected [2, 8]. All $F(m, r)$ variants of our approach maintain error levels below this threshold, thereby ensuring stable and reliable performance in practical applications.

5 RELATED WORK

Since the pioneering work of Lavin and Gray [19], who introduced the Winograd Minimal Filter Algorithm to reduce the computational complexity of convolutional operations in convolutional neural networks (CNNs), significant efforts have been devoted to optimizing Winograd-based convolution methods across diverse architectures and optimization layers. For example, Jia et al. [14] implemented an N-dimensional Winograd convolution capable of handling arbitrary kernel sizes, and optimized it for x86 many-core CPUs. Meanwhile, Li et al. [20] improved performance on ARM many-core

Table 2. Element errors of convolution neural networks.

Network	Error Type	Ours-F($2^2, 3^2$)	Ours-F($4^2, 3^2$)	Ours-F($6^2, 3^2$)	NCNN-F($2^2, 3^2$)	NCNN-F($4^2, 3^2$)
VggNet	avg	9.384078E-06	1.089130E-05	7.089612E-05	9.377054E-06	2.084713E-05
	max	1.628480E-05	3.041010E-05	1.220090E-04	1.624360E-05	3.623090E-05
FusionNet	avg	1.261121E-05	4.675881E-05	9.513018E-05	1.260211E-05	2.839505E-05
	max	3.239750E-05	1.195620E-04	2.424290E-04	3.235360E-05	7.259690E-05

		NCNN-F($6^2, 3^2$)	NNPACK	FastConv	ACL
VggNet	avg	7.023788E-05	4.903992E-05	7.914980E-05	3.513735E-05
	max	1.220840E-04	7.423270E-05	1.383230E-04	6.083400E-05
FusionNet	avg	9.406444E-05	5.613214E-05	1.176832E-04	4.370908E-05
	max	2.379180E-04	1.085370E-04	2.993280E-04	1.191110E-04

processors by integrating TEWMM and GEMM kernels, and by implementing a NUMA-aware scheduling strategy to mitigate the impact of remote memory accesses and cache contention.

Further optimization paradigms have been explored in other works. Lan et al. [17] proposed FeatherCNN, which introduced the TensorGEMM subroutine to optimize Winograd convolution by reducing memory movement and improving register blocking efficiency. Building on FeatherCNN, Meng et al. [22] proposed FastConv, which enhanced FeatherCNN by incorporating automatic kernel generation and auto-tuning strategies, allowing it to achieve better performance portability and adaptability across various ARM CPU configurations. For Intel Xeon Scalable Processor environments, Wang et al. [21, 31] demonstrated enhancements to LoWino, leveraging VNNI instructions to accelerate low-precision computations.

Substantial progress has also been made on GPU platforms. Yan et al. [34] improved single-precision Winograd convolution performance on NVIDIA Volta and Turing architectures by conducting SASS-level optimizations and refining memory access patterns. Jia et al. [13], in turn, introduced a MegaKernel-based fusion approach and a novel task mapping algorithm to reduce task dependency overheads and achieve better resource balance.

Furthermore, advances have been made to extend the applicability of the Winograd algorithm to larger kernels and more complex convolutional settings. Huang et al. [11] proposed the Decomposable Winograd Method (DWM), which decomposes large kernels into smaller ones to accommodate large kernel and stride scenarios. Similarly, Yang et al. [35] introduced the Stride-based Convolution Decomposition Method (SCDM), enabling the application of Winograd, FFT, and FFA-based accelerations over a variety of convolution sizes and strides.

Compared with solutions employing TEWMM [20] or TensorGEMM [17, 22], our method uses GEMM, which exhibits higher arithmetic intensity. By carefully designing the execution order and tuning our micro-kernels at the assembly level, we substantially reduce the strided memory access overhead incurred by GEMM-format transformations. Relative to other GEMM-based libraries [14, 21, 31], our approach introduces a novel customized data layout that further enhances computational efficiency. In contrast to the non-fused frameworks used in [14, 17, 20–22, 31], our fused framework more effectively exploits cache locality. Moreover, whereas the fused framework in [22] configures the GEMM phase through T_{blk} and K_{blk} , our method also blocks on the C dimension. This additional blocking not only improves computational efficiency but also demonstrates strong performance for larger m . Finally, we introduce a multi-dimensional parallel strategy tailored to our fused framework.

Overall, these contributions exemplify the adaptability, efficiency, and ongoing evolution of Winograd-based convolution methods across diverse hardware platforms and algorithmic landscapes. While many approaches target specific architectural features, data movement patterns, and memory hierarchies to enhance performance, other works concentrate on purely algorithmic optimizations. Collectively, these efforts continue to propel the state of the art in high-performance deep learning computations.

6 CONCLUSION AND FUTURE WORK

In this work, we introduce a fused method for efficiently implementing Winograd Convolution on ARMv8 CPUs, aiming to maximize cache locality through a fully integrated approach. We implement the core micro-kernels in AArch64 assembly, enabling architecture-specific optimizations. By employing highly optimized transformation kernels, our approach significantly reduces the overhead caused by strided memory access during data transformation into a GEMM-friendly format. A carefully designed GEMM micro-kernel, combined with a ping-pong technique and a customized data layout, maintains continuous memory access throughout computation and thus boosts throughput.

Given the unique characteristics of ConvNet dimensions, we have specifically addressed edge cases that may occur in the K and C dimensions. Furthermore, as T decreases, the overhead of handling edge cases becomes more pronounced. To address this, we provide two types of micro-kernels. While a micro-kernel with a larger α can result in reduced arithmetic intensity due to the increased occurrence of edge cases, our dual micro-kernel strategy effectively mitigates this issue.

Through a rigorous analysis, we identified optimal block parameters to further elevate performance. Additionally, we propose a novel multi-dimensional parallel strategy specifically optimized for our fused framework.

As a result, our method delivers mean speedups of 2.07 \times , 2.27 \times , 3.78 \times , and 2.07 \times over NCNN, NNPACK, FastConv, and ACL, respectively, on the Kunpeng920 under multi-threaded settings; 1.94 \times , 1.60 \times , 4.32 \times , and 2.86 \times on AWS Graviton2, and 1.93 \times , 2.00 \times , 4.14 \times , and 4.13 \times on Phytium 2000+, all evaluated across our benchmark layers. These multi-threaded results underscore the potential of our fused approach to reduce transformation overhead, enhance computational efficiency, and maintain strong parallel performance, offering a robust solution for optimizing Winograd Convolution on ARMv8 CPUs.

Looking ahead, we plan to extend our method to 3-D Winograd Convolution, which introduces greater complexity than its 2-D counterpart, and to larger filter kernels. We also intend to adapt our approach for other architectures, including x86 and RISC-V, to further broaden its applicability.

REFERENCES

- [1] Sharan Chetlur, Cliff Woolley, Philippe Vandermersch, Jonathan Cohen, John Tran, Bryan Catanzaro, and Evan Shelhamer. 2014. cuDNN: Efficient primitives for deep learning. *arXiv preprint arXiv:1410.0759* (2014).
- [2] Matthieu Courbariaux, Yoshua Bengio, and Jean-Pierre David. 2015. Low precision arithmetic for deep learning. In *ICLR (Workshop)*.
- [3] Leonardo Dagum and Ramesh Menon. 1998. OpenMP: an industry standard API for shared-memory programming. *IEEE Computational Science and Engineering* 5, 1 (1998), 46–55.
- [4] ARM Developer. 2024. *ARM NEON Intrinsic Reference*. <https://developer.arm.com/architectures/instruction-sets/simd-isas/neon/intrinsics>
- [5] Marat Dukhan. 2024. NNPACK. <https://github.com/Maratyszczka/NNPACK> Accessed: 2024-04-28.
- [6] Michele Di Giorgio. 2024. ARM Compute Library. <https://github.com/ARM-software/ComputeLibrary>. Accessed: 2024-12-02.
- [7] Kazushige Goto and Robert Van De Geijn. 2008. High-performance implementation of the level-3 BLAS. *ACM Transactions on Mathematical Software (TOMS)* 35, 1 (2008), 1–14.
- [8] Suyog Gupta, Ankur Agrawal, Kailash Gopalakrishnan, and Pritish Narayanan. 2015. Deep learning with limited numerical precision. In *International Conference on Machine Learning*. PMLR, 1737–1746.

- [9] Kaiming He, Xiangyu Zhang, Shaoqing Ren, and Jian Sun. 2016. Deep residual learning for image recognition. In *Proceedings of the IEEE Conference on Computer Vision and Pattern Recognition*. 770–778.
- [10] HiSilicon. 2019. Huawei Kunpeng 920. <https://www.hisilicon.com/en/products/Kunpeng/Huawei-Kunpeng/Huawei-Kunpeng-920>
- [11] Di Huang, Xishan Zhang, Rui Zhang, Tian Zhi, Deyuan He, Jiaming Guo, Chang Liu, Qi Guo, Zidong Du, Shaoli Liu, et al. 2020. DWM: A decomposable Winograd method for convolution acceleration. In *Proceedings of the AAAI Conference on Artificial Intelligence*, Vol. 34. 4174–4181.
- [12] Intel. 2024. oneAPI Deep Neural Network Library (oneDNN). <https://github.com/oneapi-src/oneDNN>
- [13] Liancheng Jia, Yun Liang, Xiuhong Li, Liqiang Lu, and Shengen Yan. 2020. Enabling efficient fast convolution algorithms on GPUs via MegaKernels. *IEEE Trans. Comput.* 69, 7 (2020), 986–997.
- [14] Zhen Jia, Aleksandar Zlateski, Fredo Durand, and Kai Li. 2018. Optimizing N-dimensional, Winograd-based convolution for manycore CPUs. In *Proceedings of the 23rd ACM SIGPLAN Symposium on Principles and Practice of Parallel Programming*. 109–123.
- [15] Jehandad Khan, Paul Fultz, Artem Tamazov, Daniel Lowell, Chao Liu, Michael Melesse, Murali Nandhimandalam, Kamil Nasyrov, Ilya Perminov, Tejash Shah, et al. 2019. MIOpen: An open source library for deep learning primitives. *arXiv preprint arXiv:1910.00078* (2019).
- [16] Alex Krizhevsky, Ilya Sutskever, and Geoffrey E Hinton. 2012. Imagenet classification with deep convolutional neural networks. *Advances in Neural Information Processing Systems* 25 (2012).
- [17] Haidong Lan, Jintao Meng, Christian Hundt, Bertil Schmidt, Minwen Deng, Xiaoning Wang, Weiguo Liu, Yu Qiao, and Shengzhong Feng. 2019. FeatherCNN: Fast inference computation with TensorGEMM on ARM architectures. *IEEE Transactions on Parallel and Distributed Systems* 31, 3 (2019), 580–594.
- [18] Andrew Lavin. 2024. wincnn. <https://github.com/andravin/wincnn> Accessed: 2024-03-27.
- [19] Andrew Lavin and Scott Gray. 2016. Fast algorithms for convolutional neural networks. In *Proceedings of The IEEE Conference on Computer Vision and Pattern Recognition*. 4013–4021.
- [20] Dongsheng Li, Dan Huang, Zhiguang Chen, and Yutong Lu. 2021. Optimizing massively parallel winograd convolution on arm processor. In *Proceedings of the 50th International Conference on Parallel Processing*. 1–12.
- [21] Guangli Li, Zhen Jia, Xiaobing Feng, and Yida Wang. 2021. Lowino: Towards efficient low-precision winograd convolutions on modern cpus. In *Proceedings of the 50th International Conference on Parallel Processing*. 1–11.
- [22] Jintao Meng, Chen Zhuang, Peng Chen, Mohamed Wahib, Bertil Schmidt, Xiao Wang, Haidong Lan, Dou Wu, Minwen Deng, Yanjie Wei, et al. 2022. Automatic generation of high-performance convolution kernels on ARM CPUs for deep learning. *IEEE Transactions on Parallel and Distributed Systems* 33, 11 (2022), 2885–2899.
- [23] Tran Minh Quan, David Grant Colburn Hildebrand, and Won-Ki Jeong. 2021. Fusionnet: A deep fully residual convolutional neural network for image segmentation in connectomics. *Frontiers in Computer Science* 3 (2021), 613981.
- [24] Colfax Research. 2016. FALCON Library: Fast Image Convolution in Neural Networks on Intel Architecture. <https://colfaxresearch.com/falcon-library/>
- [25] Amazon Web Services. 2024. Amazon EC2 Instances Powered by AWS Graviton Processors. <https://aws.amazon.com/ec2/graviton/>
- [26] Karen Simonyan and Andrew Zisserman. 2014. Very deep convolutional networks for large-scale image recognition. *arXiv preprint arXiv:1409.1556* (2014).
- [27] Xing Su, Xiangke Liao, Hao Jiang, Canqun Yang, and Jingling Xue. 2018. SCP: Shared cache partitioning for high-performance GEMM. *ACM Transactions on Architecture and Code Optimization (TACO)* 15, 4 (2018), 1–21.
- [28] Christian Szegedy, Wei Liu, Yangqing Jia, Pierre Sermanet, Scott Reed, Dragomir Anguelov, Dumitru Erhan, Vincent Vanhoucke, and Andrew Rabinovich. 2015. Going deeper with convolutions. In *Proceedings of the IEEE Conference on Computer Vision and Pattern Recognition*. 1–9.
- [29] Mohammad Mustafa Taye. 2023. Theoretical understanding of convolutional neural network: Concepts, architectures, applications, future directions. *Computation* 11, 3 (2023), 52.
- [30] Tencent. 2024. ncnm. <https://github.com/Tencent/ncnn> Accessed: 2024-04-12.
- [31] Xueying Wang, Guangli Li, Zhen Jia, Xiaobing Feng, and Yida Wang. 2024. Fast convolution meets low precision: Exploring efficient quantized Winograd convolution on modern CPUs. *ACM Transactions on Architecture and Code Optimization* 21, 1 (2024), 1–26.
- [32] Cunyang Wei, Haipeng Jia, Yunqian Zhang, Liusha Xu, and Ji Qi. 2022. IATF: An input-aware tuning framework for compact blas based on ARMv8 CPUs. In *Proceedings of the 51st International Conference on Parallel Processing*. 1–11.
- [33] Shmuel Winograd. 1980. *Arithmetic Complexity of Computations*. Vol. 33. Siam.
- [34] Da Yan, Wei Wang, and Xiaowen Chu. 2020. Optimizing batched winograd convolution on GPUs. In *Proceedings of the 25th ACM SIGPLAN Symposium on Principles and Practice of Parallel Programming*. 32–44.
- [35] Chen Yang, Yizhou Wang, Xiaoli Wang, and Li Geng. 2020. A stride-based convolution decomposition method to stretch CNN acceleration algorithms for efficient and flexible hardware implementation. *IEEE Transactions on Circuits and Systems I: Regular Papers* 67, 9 (2020), 3007–3020.
- [36] Weiling Yang, Jianbin Fang, and Dezun Dong. 2021. Characterizing small-scale matrix multiplications on ARMv8-based many-core architectures. In *2021 IEEE International Parallel and Distributed Processing Symposium (IPDPS)*. IEEE, 101–110.
- [37] Weiling Yang, Jianbin Fang, Dezun Dong, Xing Su, and Zheng Wang. 2021. LIBSHALOM: Optimizing small and irregular-shaped matrix multiplications on ARMv8 multi-cores. In *Proceedings of the International Conference for High Performance Computing, Networking, Storage and Analysis*. 1–14.